

THE SIGNATURE OF THE WARM HOT INTERGALACTIC MEDIUM IN WMAP AND THE FORTHCOMING PLANCK DATA.

I. SUAREZ-VELÁSQUEZ¹, F.-S. KITaura¹, F. ATRIO-BARANDELA², J. P. MÜCKET¹

Draft version April 1, 2024

ABSTRACT

We compute the cross-correlation between the Warm-Hot Intergalactic Medium and maps of cosmic microwave background temperature anisotropies using a log-normal probability density function to describe the weakly non-linear matter density field. We search for this contribution in the data measured by the *Wilkinson Microwave Anisotropy Probe*. We use a template of projected matter density reconstructed from the Two-Micron All-Sky Redshift Survey as a tracer of the electron distribution. The spatial distribution of filaments is modeled using the recently developed Augmented Lagrangian Perturbation Theory. On the scales considered here, the reconstructed density field is very well described by the assumed log-normal distribution function. We predict that the cross-correlation will have an amplitude of $0.03 - 0.3\mu\text{K}$. The measured value is close to $1.5\mu\text{K}$, compatible with random alignments between structure in the template and in the temperature anisotropy data. Using the W1 Differencing Assembly to remove this systematic gives a residual correlation dominated by Galactic foregrounds. *Planck* could detect the Warm-Hot Medium if it is well traced by the density field reconstructed from galaxy surveys. The 217GHz channel will allow to eliminate spurious contributions and its large frequency coverage can show the sign change from the Rayleigh–Jeans to the Wien part of the spectrum, characteristic of the thermal Sunyaev-Zeldovich effect.

Subject headings: cosmic background radiation - cosmology: observations - cosmology: theory - intergalactic medium

1. INTRODUCTION.

The baryon budget in the local universe shows a deficit relative to the predicted density synthesized in the big-bang (Fukugita et al. 1998; Fukugita & Peebles, 2004). Galaxies and clusters contain about 10% of the total number of baryons and an extra 5% could be in the form of circumgalactic medium (CGM) around galaxies, although the results of Gupta et al. (2012) of a large-scale massive hot gaseous halo around the Galaxy have been disputed by Wang & Yao (2012). Of the reminder 85-90%, only half has been accounted for in the low redshift intergalactic medium (Danforth & Shull 2008). Hydrodynamical simulations predict that the rest could reside within mildly-nonlinear structures with temperatures $0.01 - 1\text{keV}$, called Warm-Hot Intergalactic Medium (WHIM). The baryon fraction in this medium could be 40% (Cen & Ostriker 1999; Davé et al. 1999, 2001, Smith et al. 2011). In the X-ray, the WHIM signature has been searched both in emission and in absorption. Soltan (2006) looked for the extended soft X-ray emission around field galaxies but his task was complicated by the need to subtract all systematic effects that could mimic the diffuse signal. The recent observational effort has concentrated in searching for absorption lines due to highly ionized heavy elements from the far-ultraviolet to the soft X-ray (see Shull et al. 2012, for a review). Alternatively, as the WHIM is highly ionized, in Atrio-Barandela & Mücke (2006) and Atrio-Barandela et al. (2008) we suggested that it would generate measurable temperature anisotropies on the cos-

mic microwave background (CMB) due to the thermal and kinematic Sunyaev-Zeldovich effect (TSZ and KSZ, respectively; Sunyaev & Zeldovich 1970, Sunyaev & Zeldovich 1972). Our expectations were confirmed by Hallman et al. (2007) who found, using numerical simulations, that after the contribution of resolved clusters is removed, about one-third of the SZ flux from unresolved sources would be generated by unbound gas. More recently, Lieu & Duan (2013) suggested that the line-of-sight column density of the ionized baryons in the local universe could be determined by monitoring quasar light curves.

Our model assumes that the undetected baryon phase, in the form of filaments of hot and low density IGM, is well described by a log-normal probability distribution function. The filamentary structure of the intercluster medium has been recently confirmed using observations on interacting clusters. A joint analysis of ROSAT X-ray and Planck CMB data has provided the first detection of hot and diffuse intercluster gas, extending beyond the virial region of the cluster pair A399-A401 (Planck Collaboration, 2013). If the WHIM can be traced with templates constructed from the matter distribution, then cross-correlating those templates with CMB maps could provide further evidence of the existence of the WHIM or provide strong constraints on its spatial distribution. Based on our log-normal model, in this article we compute the cross-correlation between CMB data with a template that traces the WHIM distribution. If galaxies from the Two-Micron All-Sky Redshift Survey (2MRS) are good tracers of intergalactic gas, we can predict theoretically the amplitude of the TSZ component due to the WHIM. We compare our prediction with the cross-correlation derived from *Wilkin-*

¹ Leibniz-Institut für Astrophysik, 14482 Potsdam, Germany; isuarez,kitauro,jpmuecket@aip.de

² Física Teórica, Universidad de Salamanca, 37008 Salamanca, Spain; atrio@usal.es

son *Microwave Anisotropy Probe* (WMAP) data (Jarosik et al. 2011). We show that the cross-correlation of galaxy templates and CMB data is dominated by random alignments. The differences between channels are due to Galactic foreground residuals and instrumental noise. Planck could provide the first detection of the WHIM with our method by using the 217GHz channel to remove systematics. Briefly, in Section 2 we describe our model; in Section 3 we describe the construction of the matter templates, show that they are well describe by our log-normal formalism and compute the theoretically expected amplitude of the cross-correlation; in Section 4 we particularize our methods to a matter reconstruction of the 2MRS catalog and WMAP data and discuss the prospects of a successful detection using the forthcoming Planck data; finally, in Section 5 we present our main conclusions.

2. A LOG-NORMAL MODEL OF THE WARM HOT INTERGALACTIC MEDIUM.

In our model, baryons in the WHIM are distributed like a log-normal random field. The log-normal distribution was introduced by Coles & Jones (1991) to describe the non-linear distribution of matter in the universe. In this approximation, the number density of baryons $n_B(\mathbf{x}, z)$ is given by (Choudhury et al. 2001, Atrio-Barandela & Mückel 2006)

$$n_B(\mathbf{x}, z) = n_0(z) e^{\delta_B(\mathbf{x}, z) - \Delta_B^2(z)/2}, \quad (1)$$

where \mathbf{x} denotes the spatial position at redshift z and $|\mathbf{x}(z)|$ is the proper distance, $\Delta_B^2(z) = \langle \delta_B^2(\mathbf{x}, \mathbf{z}) \rangle$, with $\delta_B(\mathbf{x}, z)$ is the baryon (linear) density contrast, $n_0(z) = \rho_B(1+z)^3 / \mu_B m_p$ with ρ_B , m_p are the baryon density and the proton mass, respectively; finally, $\mu_B = 4/(8+5Y)$ is the mean molecular weight of the IGM and $Y = 0.24$ is the helium weight fraction. The log-normal distribution has been found to describe very well the matter statistics at scales larger than $7h^{-1}\text{Mpc}$ based on the improved Wiener density reconstruction from the Sloan Digital Sky Survey (see Kitaura et al. 2009). The linear baryon power spectrum is related to the DM power spectrum by (Fang et al. 1993)

$$P_B^{(3)}(k, z) = \frac{P_{\text{DM}}^{(3)}(k, z)}{[1 + k^2 L_{\text{cut}}^2]^2}, \quad (2)$$

where the cut-off length is the scale below which baryon density perturbations are smoothed due to physical effects like Jeans dissipation or shock heating (Klar & Mückel 2010); for the WHIM, shock heating is assumed to be the dominating process. At any given redshift the comoving scale L_{cut} is determined by the condition that the linear velocity perturbation $\mathbf{v}(\mathbf{x}, \mathbf{z})$ is equal to or larger than the sound speed $c_s = (k_B T_{\text{IGM}}(z)/m_p)^{1/2}$ at each redshift. Here m_p is the proton mass and T_{IGM} is the mean Intergalactic Medium (IGM) temperature. At redshifts $z \leq 3$, $T_{\text{IGM}} = 10^{3.6} - 10^4 \text{K}$ and its variation with redshift is small (Tittley & Meiksin, 2007). In addition, $L_{\text{cut}} \approx L_0(1+z)^{1/2}$, with L_0 a constant and if $T \simeq 10^4 \text{K}$ at present then $L_0 \simeq 1.7h^{-1}\text{Mpc}$. Hereafter, L_0 will be parameterized by T_{IGM} (see Suarez-Velázquez 2013 for details).

The number density of electrons n_e in the IGM can be obtained by assuming equilibrium between recombination and photo-ionization and collisional ionization. At temperatures in the range $10^5 - 10^7 \text{K}$ and density contrasts $\delta \leq 100$, the gas can be considered fully ionized. The two-point correlation function of the spatial variations of the electron pressure is given by

$$C(\theta) = \int_0^{z_f} \int_0^{z_f} \langle S_1(\hat{x}, z) S_2(\hat{x}', z') \rangle dz dz'. \quad (3)$$

where the integration is along lines of sight separated by an angle θ . The TSZ WHIM temperature anisotropy is $\Delta T = y_c G(\nu)$, with $y_c = k\sigma_T/m_e c^2 \int T_e n_e dl$ the Comptonization parameter along the line of sight, n_e , T_e the electron density and electron temperature, $m_e c^2$ the electron annihilation temperature, k the Boltzmann constant, σ_T the Thomson cross section, $G(\nu) = (x \coth(x/2) - 4)$, with $x = h\nu/kT_0$ the reduced frequency, T_0 the CMB temperature, dl the line element along the line of sight and dz its corresponding redshift interval. Then if $S_1 = S_2 = (k\sigma_T/m_e c^2) n_e T_e (dl/dz)$, from eq. (3) we can obtain the contribution of the WHIM to the power spectrum of CMB temperature anisotropies as

$$C_\ell = 2\pi \int_{-1}^{+1} C(\theta) P_\ell(\cos \theta) d \cos \theta \quad (4)$$

where P_ℓ is the Legendre polynomial of multipole ℓ . In Atrio-Barandela & Mückel (2006) we modeled the gas as a polytrope. The amplitude of the resulting power spectrum was strongly dependent on the polytropic index; for some model parameters, it would be larger than $100(\mu\text{K})^2$. Recently, Suarez-Velázquez et al. (2013) have refined the model for the shock-heated IGM by deriving the relation T_e versus n_e from a fit to the phase diagrams obtained in various hydrodynamical simulations. The fit $\log_{10} T_e = 8 - 2[\log_{10}(4 + x^b)]^{-1}$ with $b = \alpha + x^{-1}$ and $x = n_e/\bar{n}_B$ the electron density in units of the mean baryon density, reproduces well the phase diagram in Kang et al. (2005). Then, the model is parameterized by the IGM temperature and equation of state with parameters in the range $T_{\text{IGM}} = [10^{3.6}, 10^4] \text{K}$ and $\alpha = [1, 4]$. For this parameterization, temperature anisotropies grow with increasing electron temperature and decreasing cut-off length L_0 .

3. CROSS-CORRELATION OF MATTER DENSITY TEMPLATES AND CMB MAPS.

The search of the WHIM contribution to the temperature anisotropies of the CMB was pioneered by Hernández-Monteagudo et al. (2004). We correlated the first year of WMAP 1yr with templates of projected matter density constructed from the Two Micron All Sky Survey (2MASS) galaxy catalog; all significant TSZ contributions were originated by clusters of galaxies and no evidence of the WHIM was found. A second approach was tried by Génova-Santos et al. (2009, 2013), who used a Monte Carlo Markov Chain to find the contribution in the CMB power spectrum but the evidence was not statistically significative. In this article we revisit the cross-correlation approach using templates of the density field reconstructed from 2MRS by Kitaura et al. (2012). The reconstruction technique is based on a Bayesian Networks Machine Learning algorithm (the KIGEN-code)

which self-consistently samples the initial density fluctuations compatible with the observed galaxy distribution and a structure formation model given by second order Lagrangian perturbation theory (2LPT). We have used the Augmented Lagrangian Perturbation Theory (ALPT; Kitaura & Hess 2012) to perform constrained simulations from the initial conditions found with KIGEN. It improves previous approximations at all scales by combining 2LPT with the spherical collapse model and shows a higher correlation with the N-body solution than previous methods. This approach enables us to find non-linear structures like filaments in the cosmic web to great accuracy. The number of solutions compatible with the observations of a galaxy sample is degenerate due to shell crossing and redshift distortions and the method provides an ensemble of reconstructions useful to estimate the uncertainties associated with the technique and intrinsic to the data (see Kitaura 2012 for details). Work to perform self-consistent reconstructions implementing ALPT within the KIGEN-code is in progress (Hess et al. 2013 in preparation).

The reconstruction of the matter density field requires evaluation of FFTs and, therefore, it is carried out on a cubic box. Cubic boxes of side $160h^{-1}\text{Mpc}$ and $180h^{-1}\text{Mpc}$ were used to check that the impact of boundary effects in the density field is negligible on spheres of radius up to $80h^{-1}\text{Mpc}$. To consider even larger volumes one would require to model the “Kaiser Rocket effect” in the selection function (Branchini et al. 2012) which is beyond the scope of this work. One such reconstruction, denoted by M , is represented in Fig. 1a. The matter distribution shows well defined filaments, characteristic for the mildly non-linear regime. The sky is represented using Healpix (Gorski et al. 2005) with resolution $N_{\text{side}} = 128$, that corresponds to an angular resolution of $27.5'$. We used a linear scale saturated at 500 galaxies per pixel for better visualization. In Fig. 1b we represent the difference between two reconstructions. While the cosmic web displayed in all reconstructions is very similar, the extension around very massive structures and the exact location of filaments differ from one reconstruction to another. For example, the uncertainty on the position of Coma is $2 - 3h^{-1}\text{Mpc}$, less than 5% of its distance to the Local Group. Filaments that are slightly displaced appear in the difference map to be running side by side. The ensemble of constrained simulations can be used to compute the mean and standard deviation of the density field in each cell, giving an estimate of the uncertainty in the position of the density peaks and filaments. For illustration, in Fig. 1c we represent the W1 Differencing Assembly of WMAP 7yr data. The galactic and point source contaminations are masked using the extended temperature analysis WMAP mask KQ75. The data is normalized to zero mean and unit variance outside the mask.

In Fig. 2 we represent the mean power spectra of 24 different template reconstructions of the matter distribution like in Fig. 1a that are compatible with 2MRS (solid blue line) and the rms dispersion around the mean (shaded area). The dot-dashed (green) line represents the power spectrum of the projected density of 2MASS galaxies used in this reconstruction, corrected by inverse weighting with the selection function. To avoid the instabilities due to small divisors, 37 pixels with number

density of galaxies equal to or larger than 10^3 galaxies were eliminated. All templates were normalized to zero mean and unit variance. Since the projected distribution of galaxies is close to a Poisson point process, the power spectrum of 2MASS galaxies is roughly constant and very different, at high multipoles, from the spectrum of the reconstructed matter density field. At those scales, the matter distribution is smoother and the power falls. The solid red line represents the power spectrum of the baryon density distribution computed by taking $S_1 = S_2 = n_e$ in eq. (3), with a cut-off length of $L_0 \simeq 1.13h^{-1}\text{Mpc}$. We found that the best fit to the power spectrum of the reconstructed template was obtained when the integration in eq. (3) was restricted to the interval $60 - 120h^{-1}\text{Mpc}$, while the template of Fig. 1a reproduces the local volume out to $80h^{-1}\text{Mpc}$. This discrepancy is only apparent. Even if the template has been reconstructed up to $80h^{-1}\text{Mpc}$, it does include higher modes since the method uses a $160h^{-1}\text{Mpc}$ box. Second, we have to take into account sampling variance; the local universe lacks power up to $30h^{-1}\text{Mpc}$ (see e.g. Courtois et al. 2012). Spikes and oscillations in the spectra reflect the sample variance associated with observing a single universe. *While the distribution of the WHIM and matter is different from that of galaxies at small scales, they coincide at large scales, as it could be expected if galaxies traces the overall matter distribution.* In the inset we represent in a logarithmic scale the power spectrum at low multipoles to show that the reconstructed matter density field and the galaxy distribution on those scales are very similar. Lines follow the same convention that in the main plot. To facilitate the comparison, the power spectrum of galaxies in this inset was multiplied by a factor of 20 to bring its amplitude closer to that of the power spectrum of the reconstructed matter density templates.

Except at very large scales, where the power spectrum is dominated by a few modes and sample variance is large, the templates of the reconstructed matter density field agree with the log-normal model at all angular scales. This agreement demonstrates that templates like the one shown in Fig. 1a are very well described by our log-normal model, but it does not prove that the WHIM is stored in filaments. It only indicates that we can use the log-normal model to predict the value of observable quantities that can be later compared with the data. To this purpose, electron overdensities will be normalized to unit variance so the cross-correlation is given in units of temperature. For the template of Fig. 1a and for model parameters in the fiducial ranges $T_{IGM} = [10^{3.6}, 10^4]\text{K}$ and $\alpha = [1, 4]$ the correlation at the origin is $0.03 - 0.3\mu\text{K}$. For a different parameterization that fits the Cen & Ostriker (2006) phase diagram, the amplitude would be $0.01\mu\text{K}$, slightly lower.

Contributions coming from gas in clusters or in the CGM are not included in our formalism. First, the log-normal model is restricted to overdensities $\delta \leq 100$, while in clusters and in the CGM are $\delta \sim 500 - 1000$ (Fukugita & Peebles, 2004). Second, the distribution of galaxies or clusters is not well described by our log-normal model. For instance, the CGM would induce anisotropies with the spatial distribution of galaxies and not filaments that, as Fig. 2 shows, are very different.

If a template M is a good tracer of the gas in filaments, cross-correlation with CMB data will give us an estimate of the CMB temperature anisotropies generated by the WHIM measured, for example, by WMAP. Since the reconstruction is not unique, we need to quantify the uncertainty introduced by using a template that does not exactly describe the distribution of baryons. To speed up the calculation we degraded all our templates to a resolution of $\sim 1.8^\circ$, corresponding to Healpix $N_{\text{side}} = 32$. At this resolution, at separation of 1° the correlation function is between first neighbors, at 2° between second neighbors, etc. In Fig. 3 we represent the cross-correlation of the template M with the 24 different reconstructions of the matter density field from 2MRS. The solid (black) line represents the autocorrelation function of M ; the dashed (blue) line represents the mean of the cross-correlation of M with the other 23 different reconstructions and the shaded area is the rms dispersion about the mean. At the origin, the autocorrelation function and the mean of the cross-correlations differ by 20%. Outside the origin, the autocorrelation is similar to the mean and very well within the 1σ error bar, indicating that the uncertainty on the position of the density peaks in the matter reconstruction of the 2MRS catalog is $\sim 2^\circ$. Fig. 3 is very illustrative of the accuracy of our method. Using resolution $N_{\text{side}} = 32$ instead of $N_{\text{side}} = 128$ we lose information about the correlation on scales $0.5^\circ - 2^\circ$, but on those scales the reconstruction of the density field is uncertain (see Fig 1b). If we use a reconstruction of the density field that is not fully coincident with the true distribution of baryons in the local universe, we can expect to underestimate the true correlation function by the 20% but the effect is negligible outside the origin. Then, by restricting our analysis to Healpix resolution $N_{\text{side}} = 32$ not only the computation is faster, we also average over the uncertainties on our template that only contribute with a 20% uncertainty on the correlation at zero lag. With this resolution there are no differences between WMAP 7yr and 9yr data and the former were used.

4. APPLICATION TO WMAP DATA

Since the log-normal model describes reasonably well the power spectrum of the matter density then cross-correlation of a matter template M with WMAP 7yr data would determine the fraction of gas traced by the matter. In Fig. 4a we represent the cross-correlation of M with the eight DAs of WMAP 7yr data. From top to bottom: solid (blue), dashed (green) and dot-dashed (red) lines correspond to the Q, V and W channels. The contribution of galactic foregrounds and point sources were removed using the KQ75 mask that eliminates 27% of the sky (see Fig 1c). The matter density template M was normalized to zero mean and unit variance *outside the mask*. The symmetric solid (black) lines represent the rms deviation of the cross-correlations of M with 1,000 different random realizations of WMAP data that include cosmological CMB signal and noise, but no foreground residuals. The amplitude of the cross-correlation at the origin, $\sim 1.5\mu\text{K}$, is much larger than the expected amplitude of $0.03 - 0.3\mu\text{K}$ and it is compatible with being due to random alignments between structures in the CMB data and in the template. The differences between the eight DA are due to the WHIM, noise and

foreground residuals. Subtracting the correlation of M and W1 to the correlation of M with the other seven DA removes the contribution due to random alignments and yet, due to the frequency variation of the TSZ from 40 to 90 GHz, it leaves 14-18% of the original TSZ signal in the V and Q bands, respectively. If in Fig 4a the differences were dominated by TSZ, then the quantity $\langle (T - W1)M \rangle = [C_{\nu,M} - C_{W1,M}]/[G(\nu) - G(W1)]$ would give the correlation of the template with the map of the Comptonization parameter, y_c -map. In Fig 4b we plot the $\langle M(y_c - \text{map}) \rangle$ correlation for WMAP. The solid (blue) and dashed (green) lines corresponds to the Q and V channels, respectively. The differences between the W2, W3, W4 DA with W1 would remove not only the intrinsic CMB, but also the foreground and WHIM signals. The rms variation of the subtracted correlations of the W channel provides a simple estimate of the error bar due to the instrumental noise, but does not account for foreground residuals and sampling variance contributions due to the variation of the number of pairs with separation angle. The error bars are represented in Fig. 4b by the symmetrical solid (black) lines. The correlations $\langle (Q_{1,2} - W1)M \rangle$ and $\langle (V_{1,2} - W1)M \rangle$ are similar and well outside the error bar, *but this is not evidence of WHIM*. In fact, the $\langle M(y_c - \text{map}) \rangle$ correlation should be positive at the origin, not negative. We verify that this residual correlation is due to foregrounds by masking all CMB data with $|b| \leq 30^\circ$. The results are presented in Fig. 4c. Lines follow the same convention as in the panel (b). By restricting the correlation to the polar caps, $\langle (Q_{1,2} - W1)M \rangle$ decreased by 30% while $\langle (V_{1,2} - W1)M \rangle$ became positive, with an amplitude of $0.4\mu\text{K}$ at the origin, compatible with noise. Compared with Fig. 4b, the correlation of the Q and V band are very different, reflecting the differences in the foreground residuals between the $Q - W1$ and the $V - W1$ maps and an increased sample variance as the fraction of the sky removed was larger.

The previous results indicate that WMAP is not well suited to separate the TSZ contribution from that of the other components. In this respect, Planck is a much better instrument. To forecast its performance, we simulated 6 Planck channels with frequencies in the range 44 – 353GHz. The simulated maps were constrained to reproduce WMAP data for multipoles $\ell \leq 256$. The maps were downgraded to resolution $N_{\text{side}} = 32$ so differences in beamwidth and beam asymmetries have an unmeasurable effect. The simulated data contain CMB and homogeneous white noise but did not contain foregrounds, foreground residuals or $(1/f)$ noise. At each frequency we added a WHIM component following the matter distribution in M assuming $T_e \propto n_e$ with a mean Comptonization parameter $\langle y_c - \text{map} \rangle = 0.1\mu\text{K}$. In the frequency range considered, the amplitude of TSZ effect varies from -1.9 at 44GHz to 2.2 at 353 GHz and passes through the TSZ null at 217GHz. This channel was later used to subtract the correlation of M with the CMB data due to random alignments. In Fig. 4d we plot the results (solid black line), that are very close to each other and close to the theoretical expectation, represented by the dashed (blue) line. The differences between the theoretical curve and the simulated data are due to masking and pixelization. If foreground and noise inhomogeneities are not important and the template traces the gas distribu-

tion, Planck will measure the WHIM TSZ correlation very accurately.

Together with the uncertainties in the reconstruction of the density field, there are additional uncertainties associated with how well the galaxy template traces the electron pressure. The WHIM could be made of clumps, with typical sizes $100h^{-1}\text{Kpc}$ like the CGM. At $60h^{-1}\text{Mpc}$, a clump of this size would subtend $6'$. The 217 and 343GHz Planck channels have the largest resolution of the instrument, $5'$; then, in Planck data we can neglect the effect of gas inhomogeneities at scales below $100h^{-1}\text{Kpc}$. Also, in our analysis we have assumed a smooth distribution of baryons and temperatures within the filaments. As an average of the different Kang et al. (2005) models we assumed the temperature scaling as $T_e \propto n_e$ so the electron pressure in the template scaled as $n_e T_e \propto n_e^2$. The simulations of individual filaments carried out in Klar & Mücke (2010, 2012) have characterized the state of the gas and its evolution inside the filament in terms of the length of the initial perturbation. Their simulations indicated the existence of multiple phases and temperatures in the WHIM. To estimate the uncertainty associated with an inhomogeneous distribution of gas and temperature within filaments, we repeat our simulations but added to the CMB data a TSZ contribution with two different temperature scalings in the range $\delta \in [1, 100]$: (1) an isothermal gas $T \sim \text{const}$ and (2) a clumpier temperature distribution, $T_e \propto n_e^2$. In both cases, the mean amplitude of the y_e -map was $0.1\mu\text{K}$. These temperature-density relations can be considered extreme cases of the temperature variation in the IGM. Next, we cross correlate the CMB data with our template M , where the electron pressure scales like $n_e T_e \propto n_e^2$. The resulting correlations are represented by dot-dashed (red and violet) lines in Fig 4d. The comparison of these cross-correlations with our previous result shows that, at $N_{\text{side}} = 32$ resolution, the shapes are similar and only differ by $\sim 5\text{--}10\%$ in the amplitude at the origin. In summary, the uncertainty on the cross-correlation of template and CMB data due to (1) how the template traces the gas distribution and (2) how the electron pressure scales with density within the template add at most an uncertainty of 30% at the origin, being almost negligible on scales above 2° .

The final error bar will certainly have non-zero contributions from foreground residuals, whose distribution and amplitude change with frequency, and instrumental $(1/f)$ noise that will complicate the detection. However, first and foremost, the TSZ has a distinctive signature, different from that of any other foreground. It changes sign from the Rayleigh-Jeans to the Wien part of the spectrum. This change of sign will also be present in the correlation function, and could be sufficient to detect the effect. Second, foregrounds residuals are probably largest close to the galactic plane, so computing the cross-correlation at different galactic latitudes could help to disentangle the different contributions, as for WMAP data. Third, in our Planck simulations, the template contributes with just $0.1\mu\text{K}$. According to our model, this is a reasonable expectation for a large fraction of the parameter space. Naturally, the contribution due a larger volume will be higher so templates constructed from deeper galaxy surveys would give statistically more

significant detections.

5. CONCLUSIONS.

We have computed the amplitude of the correlation between the WHIM with CMB data. We have shown that templates of projected matter density that describe the weakly non-linear regime are well represented by our log-normal model. This permits us to predict that the amplitude of the cross-correlation of the WHIM with CMB data is $0.03\text{--}0.3\mu\text{K}$ depending on model parameters. Assuming that the reconstructed matter density templates trace the electron distribution, we computed the cross-correlation of the matter density field within a volume of $160h^{-1}\text{Mpc}$ reconstructed using the 2MRS galaxy survey. The cross-correlation with WMAP data showed it to be dominated by random alignments of CMB structures and galaxy filaments. The differences between DA could be due to the WHIM signal, but also to noise and foreground residuals. We checked that foreground residuals are the most likely source of the correlation by showing the results varied significantly when removing data with $|b| \leq 30^\circ$.

Using 2MASS galaxies and WMAP data, Lavaux et al. (2013) described evidence that baryons are distributed in galactic coronae. This result is in apparent contradiction with Hernández-Montegudo et al. (2004) where cross-correlation of WMAP 1yr data with templates of projected galaxy density showed no evidence of ionized gas outside known clusters of galaxies and, to some degree, with the results presented here. Even if our matter density templates are different from a pure galaxy template their power spectra overlap (see Fig 2) and any signal traced by galaxies must also be traced at some level by our templates. In addition, the contribution due to random alignments, that we have shown to be dominant for WMAP, was not quantified. Due to the difference in methodology, our results are not fully comparable and consistency between both methods will increase the statistical significance of any detection.

Planck, with its large frequency coverage and high resolution is a more adequate instrument than WMAP to search for the WHIM contribution. First, the 217GHz channel is very close to the TSZ null, allowing to remove spurious correlations that dominates the signal. Second, the instrument contains measurements on the Rayleigh-Jeans and Wien part of the spectrum. If the correlation is due to the WHIM, it will vary with frequency and change sign. Reconstructions of the matter density field using deeper surveys like the Sloan Digital Sky Survey will allow to probe the baryon distribution to higher depths, enhancing the signal. Alternatively, the reconstructed density field allows to select filaments aligned with the line of sight, where the optical depth of the WHIM would be larger. The higher resolution of Planck could facilitate to identify the WHIM signal in those regions and clarify its spatial distribution, whether it is distributed as a network of filaments or is stored in the galactic coronae.

I.S.V. thanks the DAAD for the financial support, grant A/08/73458. F.S.K. is a Karl-Schwarzschild fellow at the AIP. F.A.B. acknowledges financial support from the Spanish Ministerio de Educación y Ciencia (grants

FIS2009-07238, FIS2012-30926 and CSD 2007-00050).

He also thanks the hospitality of the Leibniz-Institut für Astrophysik in the early stages of this work.

REFERENCES

- Atrio-Barandela, F., & Mückel, J. P. 2006, *ApJ*, 643, 1
Atrio-Barandela, F., Mückel, J. P., & Génova-Santos, R., 2008, *ApJL*, 674, L61
Branchini, E., Davis, M. & Nusser, A., 2012, *MNRAS*, 424, 472
Cen, R., & Ostriker, J. P. 1999, *ApJL*, 519, L109
Cen, R., & Ostriker, J. P. 2006, *ApJ*, 650, 560
Choudhury, T. R., Padmanabhan, T., & Srianad, R., 2001, *MNRAS*, 322, 561
Coles, P., & Jones, B. J. T. 1991, *MNRAS*, 248, 1
Courtois, H. M., Hoffman, Y., Tully, R. B. & Gottlöber, S. 2012, *ApJ*, 744, 43
Danforth, C. W., & Shull, J. M. 2008, *ApJ*, 679, 194
Davé, R., Cen, R., Ostriker, J. P., et al. 2001, *ApJ*, 552, 473
Davé R., Hernquist, L., Katz, N. & Weinberg, D. H. 1999, *ApJ*, 511, 521
Fang, L. Z., Bi, H., Xiang, S., & Börner, G. 1993, *ApJ*, 413, 477
Fukugita, M., Hogan, C. J., & Peebles, P. J. E. 1998, *ApJ*, 503, 518
Fukugita, M., & Peebles, P. J. E. 2004, *ApJ*, 616, 643
Génova-Santos, R., Atrio-Barandela, F., Mückel, J. P., & Klar, J. S. 2009, *ApJ*, 700, 447
Génova-Santos, R., Suarez-Velázquez, I., Atrio-Barandela, F. & Mückel, J. P., 2013, *MNRAS*, in press (arXiv:1304.2901)
Gorski, K. M., Hivon, E., Banday, A. J., et al. 2005, *ApJ*, 622, 759
Gupta, A., Mathur, S., Krongold, Y., Nicastro, F. & Galeazzi, M. 2012, *ApJL*, 756, L8
Hallman, E. J., O'Shea, B. W., Burns, J. O., et al. 2007, *ApJ*, 671, 27
Hernández-Monteagudo, C., Génova-Santos, R. & Atrio-Barandela, F. 2004, *ApJL*, 613, L89
Jarosik, N., Bennett, C. L., Dunkley, J., et al. 2011, *ApJS*, 192, 14
Kang, H., Ryu, D., Cen, R. & Song, D. 2005, *ApJ*, 620, 21
Kitaura, F.-S. 2012, *MNRAS*, 420, 2737
Kitaura, F.-S., Erdogdu, P., Nuza, et al. 2012, *MNRAS*, 427, L35
Kitaura, F.-S. & Hess, S. 2012, *MNRAS* submitted (arXiv:1212.3514)
Kitaura, F.-S., Jasche, J., Li, C., et al. 2009, *MNRAS*, 400, 183
Klar, J. S. & Mückel, J. P. 2010, *A&A*, 522, 114
Klar, J. S. & Mückel, J. P. 2012, *MNRAS*, 423, 304
Lavaux, G., Afshordi, N. & Hudson, M. J. 2013, *MNRAS*, 430, 1617
Lieu, R. & Duan, L. 2013, *ApJL*, 763, L44
Planck Collaboration, Ade, P.A.R., Aghanim, N., Arnaud, M. et al. 2013, *A&A*, 550, A134
Soltan, A. M. 2006, *A&A*, 460, 59
Shull, J. M., Smith, B. D., & Danforth, D. W. 2012, *ApJ*, 759, 23
Smith, B. D., Hallman, E., Shull, J. M., & O'Shea, B. 2011, *ApJ*, 731, 6
Suarez-Velázquez, I. F., Mückel, J. P., & Atrio-Barandela, F. 2013, *MNRAS*, in press (arXiv:1303.5623)
Sunyaev, R. A., & Zel'dovich, Y. B. 1970, *ApSS*, 7, 3
Sunyaev, R. A., & Zel'dovich, Y. B. 1972, *CoASP*, 4, 173
Tittley, E., & Meiksin, A. 2007, *MNRAS*, 380, 1369
Wang, Q. D. & Yao, Y. 2012, arXiv:1211.4834

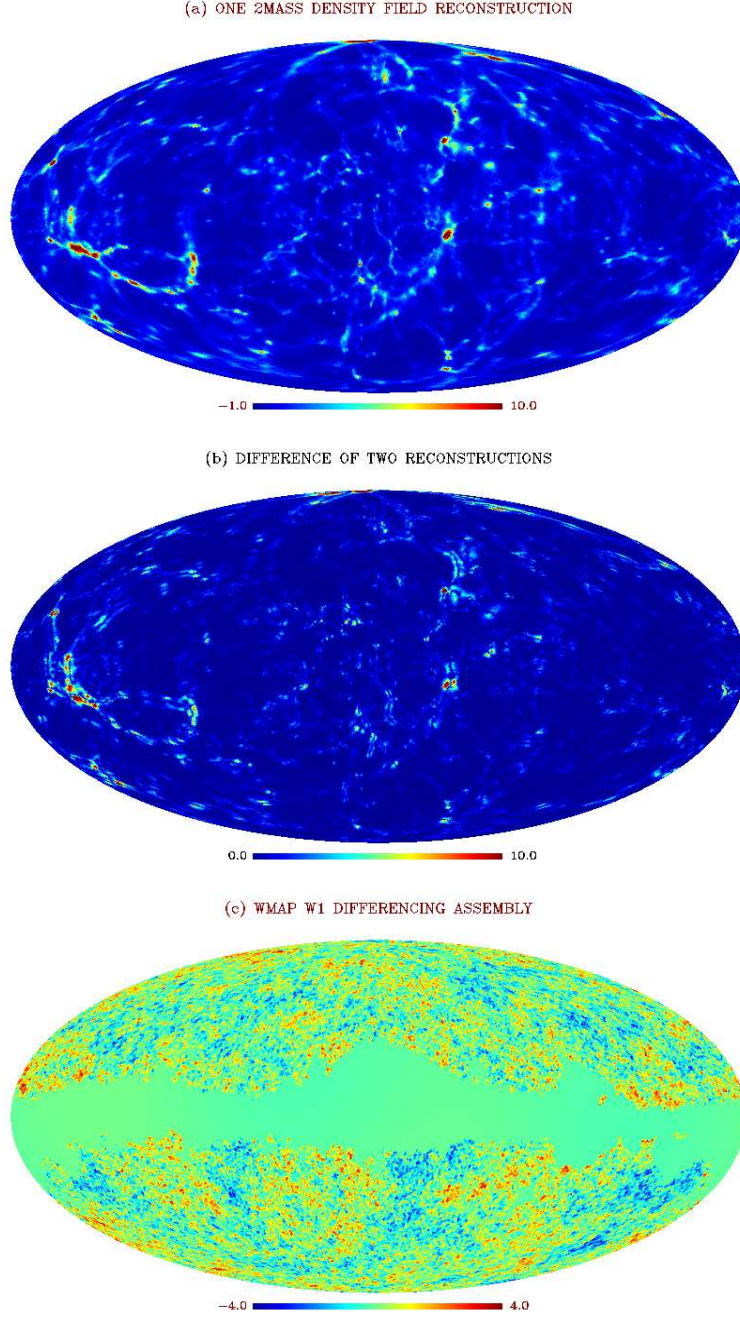


FIG. 1.— Templates and CMB data at Healpix resolution $N_{side} = 128$. (a) Template M of projected matter density reconstructed from the 2MASS catalog, showing the filamentary structure characteristic of the weakly non-linear regime. (b) Difference of two reconstructed density fields showing small displacements in the location of filaments and on the extent of massive structures. (c) WMAP data of the W1 Differencing Assembly normalized to zero mean and unit variance; the galactic plane has been masked using the KQ75 galactic and point source mask.

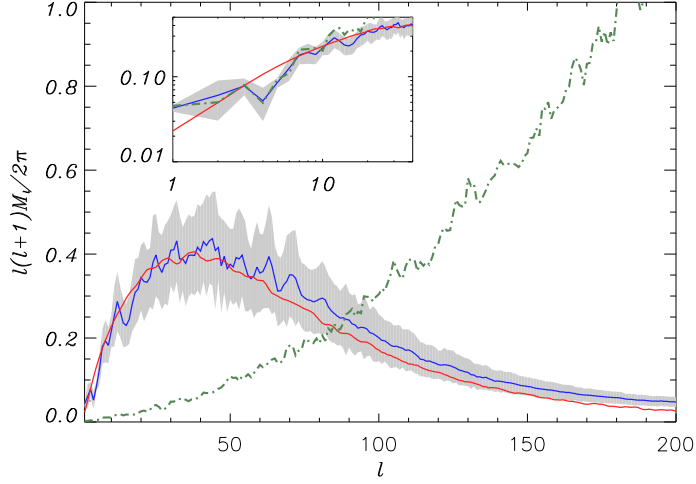


FIG. 2.— Mean power spectra of the 24 reconstructed matter distribution templates including the one represented in Fig 1a (solid blue line) and rms dispersion around the mean (shaded area). The dashed (green) line is the power spectrum of the density of 2MASS projected galaxies corrected by the selection function and the solid (red) line is the spectrum of baryon distribution given by our log-normal model. All power spectra were normalized to zero mean and unit variance. In the inset we represent the low order multipoles in a log-scale; the amplitude of the power spectrum of galaxies has been multiplied by a factor 20 to facilitate the comparison.

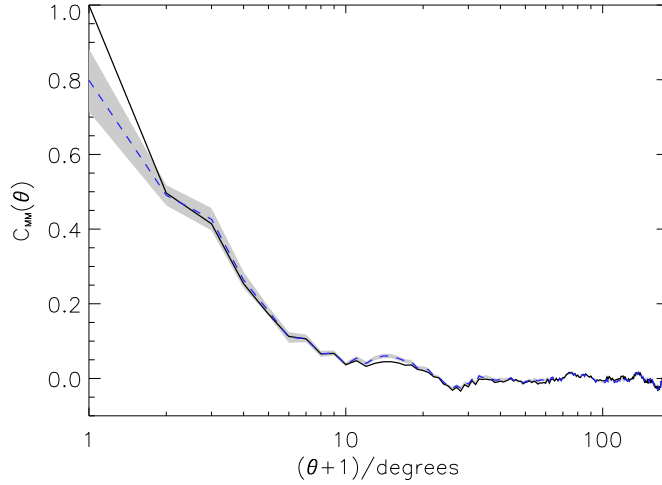


FIG. 3.— Cross-correlation of the different reconstructions of the matter density field. The autocorrelation of the template M of Fig 1a is represented by the solid (black) line while the blue dashed line and shaded area represents the mean and rms dispersion of the cross-correlation of M and the other 23 different reconstructions. For convenience, the values on the X-axis have been shifted by one degree.

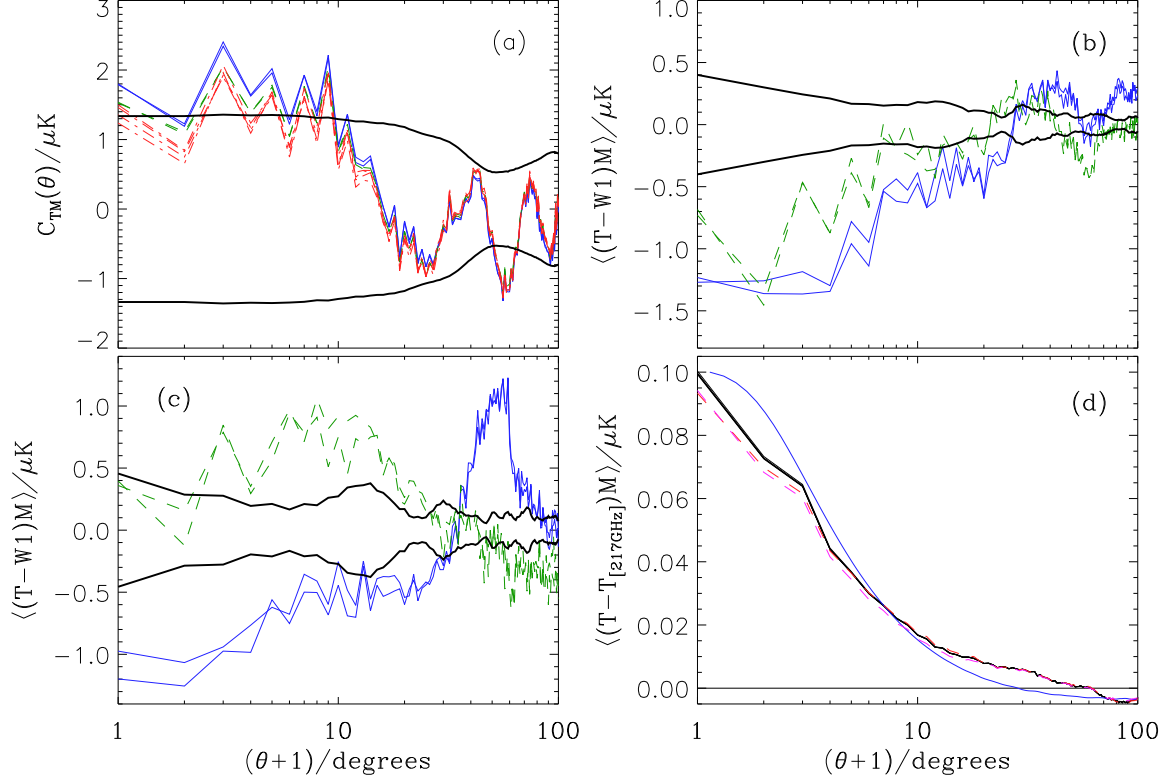


FIG. 4.— (a) Cross correlation of the template M , represented in Fig. 1a, with the 8 DA of WMAP 7yr data. From top to bottom, the solid (blue), dashed (green) and dot-dashed (red) lines correspond to the Q, V and W channels. The symmetric solid black lines correspond to the rms cross-correlation of the template with 1000 randomly generated W1 maps. (b) Cross-correlation of the Q (solid, blue) and V (dashed, green) channels after subtracting the W1 cross-correlation, renormalized to account for the removed TSZ contribution, i.e., $\langle (T-W1)M \rangle = [C_\nu(\theta) - C_{W1}(\theta)]/[G(\nu) - G(W1)]$. Black lines represent the rms of the W2, W3, W4 DA after subtracting the W1 cross-correlation. (c) As in (b) but the CMB-template correlation was computed only on pixels with $|b| \geq 30^\circ$. (d) Planck forecast: Solid (black) lines represent $\langle (T-T_{217\text{GHz}})M \rangle = [C_\nu(\theta) - C_{217\text{GHz}}(\theta)]/[G(\nu) - G(217\text{GHz})]$ for the 44-353GHz channels; the dashed (blue) line is the log-normal prediction. The dot-dashed lines (red and violet) represent the cross-correlations of the template M with Planck simulated data containing a TSZ WHIM contribution with $T_e \propto \text{const}, n_e^2$ in the range $\delta \in [1, 100]$, respectively. Like in Fig 3 the x-axis has been shifted by one degree.